ELSEVIER

Journal of Molecular Structure: THEOCHEM 762 (2006) 49–56

THEO CHEM

www.elsevier.com/locate/theochem

Structure of 55-atom bimetallic clusters

Min Zhang, René Fournier *

Department of Physics, York University, Toronto, Ont., Canada M3J 1P3

Received 17 July 2005; accepted 22 August 2005
Available online 18 January 2006

Dedicated to Annick Goursot on the occasion of her 60th birthday.

Abstract

We studied the structure of bimetallic clusters with 55 atoms having the basic geometry of a Mackay icosahedron. The energy of the clusters is calculated as a sum of pairwise Morse functions, which is a purely covalent term, plus the electrostatic energy of screened atomic charges obtained through the electronegativity equalization (EE) method. The parameters D_e, R_e, and a_e of the Morse functions vary according to the atoms' coordination and interpolate smoothly between the known (experimental) diatomic and bulk limits. The EE parameters are fitted to density functional theory ionization energies of small model clusters. The energy of the clusters $A_nB_{(55-n)}$ ($x = 13$ and 27, and A,B = Cu,Ag, and Au) was minimized with respect to site occupancy by atoms of each type by combined simulated annealing and conjugate gradient optimization. The lowest energy structures are characterized by: (i) segregation of the metal with lowest surface energy to the surface of the cluster; (ii) occupancy of the atom-capping surface sites (sites with a coordination of 6) by the lowest cohesive energy metal; (iii) a tendency toward AB ordering, to maximize ionic interactions, at the surface of AuAg and AuCu clusters; (iv) a compromise between mixing and surface segregation in some of the CuAu and AuAg clusters.

Keywords: Alloy clusters; Surface segeration; Electonegativity eualization; Empirical potential; Simulated annealing

1. Introduction

Small metallic particles are an important class of catalysts [1]. Bimetallic particles are particularly interesting [2]. Their properties are different from those of the constituent pure metals, and in many cases their catalytic activity is superior to either of them [3–5]. This has been described as a 'synergy' between the two active metals, but it is not clear what structural and electronic factors are responsible for the enhanced selectivity and activity of specific bimetallic catalysts. It appears that some catalytic reactions require ensembles of surfaces atoms having specific coordinations [6]. For ammonia synthesis, Jacobsen et al. suggest that the best catalysts are those with a N_2 adsorption energy falling within a narrow range, and that this can be achieved with two metals having an optimal interpolated value. But these authors also point out that the mixed-metal catalysts should have both metals present in close proximity at the surface in order to be effective. Therefore, it is important to know the chemical composition and structure at the surface of bimetallic clusters to understand their properties. Even if the composition of a bimetallic particle A_xB_y and the structures of the pure metal particles $A_{(x+y)}$ and $B_{(x+y)}$ were known precisely, determining the surface structure of A_xB_y would remain problematic. The surface of metal alloys have compositions that are different from the bulk; and metals that are not miscible in the bulk can form alloy like structures in sufficiently small particles [2]. Simple thermodynamic models [7] and first-principles energy calculations on model systems [8] predict an enrichment in the top layer in the metal having the lowest surface energy (segregation). But these theories assume a dilute alloy or a structureless model and cannot give detailed structural information. Furthermore, in the smallest bimetallic particles, those with diameter in the 1–3 nm range roughly [5], the surface composition is most likely a function of particle size and cannot be described by any simple model. The combination of density functional theory (DFT) and the cluster expansion (CE) method is very promising for studying the structure of binary solids and surfaces in macroscopic systems [9], but small particles with arbitrary structures (i.e. not necessarily fragments of fcc or bcc) are probably beyond the limits of this approach.

* Corresponding author. Address: Department of Chemistry, York University, 4700 Keele Street, Toronto, Ont., Canada M3J 1P3.Tel.: +1 416 736 2100; fax: +1 412 736 5936.
E-mail address: renef@yorku.ca (R. Fournier).

0166-1280/$ - see front matter © 2005 Elsevier B.V. All rights reserved.
doi:10.1016/j.theochem.2005.08.042

Detailed atomistic models could help answer some questions about the surface structure of bimetallic particles in the size range from 1 to 3 nm roughly. To what degree do the two metals mix? To what degree is the surface enriched in the metal with lower surface energy? What is the effect of size mismatch between the two elements? How do these things depend on particle size, expressed as the fraction of atoms located at the surface (dispersion)? How does temperature affect structure? Are there structural motifs that are associated only with certain sizes and compositions?

To begin answer some of these questions we studied a few bimetallic clusters in the series A_nB_{55-n}. It has been hypothesized that small metal clusters adopt icosahedral shapes because these are the most compact shapes possible and they should minimize surface energy. There is limited experimental information on the structure of 13-atom metal clusters, but studies suggest that some elements favor the icosahedral structure [10,12] and others do not [11,12]. In clusters that are so small, the effect on energy of orbital symmetry and other aspects of electronic structure can overcome the lower surface energy of the icosahedron and favor other structures. There is stronger evidence for icosahedral clusters in the size range from 40 to 200 atoms roughly [13,14]. In clusters with more than 200 atoms, it appears that icosahedra compete with Marks decahedra and crystal fragments [15] which must eventually predominate. After 13 atoms, the next perfect icosahedron in the atomic shell model occurs at 55 atoms [16]. At this larger size, the surface energy becomes a more important factor, so we expect the 55-atom Mackay icosahedron is one of the lowest energy structures, if not the global minimum, for many metallic elements. So we restrict our study to clusters with an overall icosahedral structure. This simplifies things tremendously, but we still have to tackle a minimization problem of great complexity. If we label each site of the Mackay icosahedron by an index $j=1,55$, we have to minimize the energy of A_nB_{55-n} with respect to the discrete choice of n distinct numbers j_1, j_2,…j_n, chosen among 55. The configuration space is slightly smaller than $55!/(n!\ (55-n)!)$ because of symmetry, but the number of possibilities is still enormous, there is on the order of 10^{11} substitutional isomers of $A_{13}B_{42}$ for instance. It is not possible to tackle such a problem with accurate first-principles methods because energy evaluations require too much computer time, and also because reaching self-consistent field (SCF) solutions at every step of the optimization process is an extremely difficult problem for metal particles of that size. First-principles studies were done on Ti_{55} by Wang et al. [30] and on a few Au_n clusters with n as large as 147 by Häberlen et al. [31]. Those involved only local optimization, so the number of energy evaluations required were probably on the order of 10^3, which is several orders of magnitude smaller than what is needed for global optimization of A_nB_{55-n}. Note also that the computing time required in such calculations is reduced by using the high symmetry of the clusters. This would not be possible for the vast majority of A_nB_{55-n} cluster configurations because they have no symmetry at all. On the other hand, there are many studies, including simulations and extensive optimizations, that used empirical potentials [32] for elemental clusters with 55 or more atoms and, in fewer cases, cluster alloys (for example, [23]). Here we use an empirical energy function that is a sum of a purely covalent term and a purely electrostatic term. The covalent part is described by Morse functions, and the electrostatic term is a sum of screened Coulombic interactions between atomic charges obtained in the EE model. The next section describes our computational method. In Section 3 we show the results and discuss structural trends among a few clusters A_xB_y: (a) the six combinations possible with $x=13$ and A and B chosen among Cu, Ag, Au; (b) $Cu_{27}Ag_{28}$, $Au_{27}Ag_{28}$, and $Cu_{27}Au_{28}$. We summarize and give some conclusions in Section 4.

2. Computational method

2.1. Scaled Morse potential

The Morse function [17] describes adequately the energy–distance curve of homonuclear diatomics:

$$D(r;D_e,R_e,a_e)=D_e[e^{-2a_e(r-R_e)}-2e^{-a_e(r-R_e)}] \tag{1}$$

It also describes the cohesive energy curve of bulk solids near the minimum [18]. Of course, parameters for the diatomic and bulk differ a lot. For a number of elements, including Cu, Ag, and Au, we obtained six parameters by fitting to the spectroscopic constants R_e, D_e, and a_e of the homonuclear diatomic molecule [27], and then making another fit to the nearest-neighbor distance, R_{nn}, cohesive energy, and bulk modulus of the solid [28]. In the scaled Morse potential (SMP), we interpolate between these two limits by assuming a power law for the Morse parameters and obtain a covalent bonding energy U_{cov} as a sum of pairwise interactions:

$$U_{cov}=\sum_{i>j}U_{ij}=\sum_{i>j}D(r_{ij};R_{ij},D_{ij},a_{ij})\times f(r_{ij}) \tag{2}$$

$$D_{ij}=\frac{(D_i+D_j)}{2};\quad R_{ij}=\frac{(R_i+R_j)}{2};\quad a_{ij}=\frac{(a_i+a_j)}{2} \tag{3}$$

$$D_i=D_e n_i^{\alpha};\quad R_i=R_e n_i^{\beta};\quad a_i=a_e n_i^{\gamma} \tag{4}$$

$$n_j=\sum_{i\neq j}f(r_{ij}) \tag{5}$$

$$f(r)=\begin{cases}1 & r\le C_1\\ 0 & r\ge C_2\\ \dfrac{1}{2}-\dfrac{1}{2}\sin\left[\dfrac{\pi(r-R_{mid})}{C_2-C_1}\right] & C_1<r<C_2\end{cases} \tag{6}$$

where we take $C_1=R_{nn}$ and $C_2=1.4\times R_{nn}$. We assign Morse parameters D_i, R_i, a_i to each atom i based on how many neighbours (n_i) it has. We describe the $i-j$ interaction by a Morse function with parameters averaged over the two atoms.

This idea comes from the observation that the coordination in an elemental fcc solid is 12, and it turns out that, for *s*-valence metals, D_{12} is nearly equal to $D_1 \div \sqrt{12}$. Generally, experimental and theoretical interaction energies for several metallic systems suggest a simple scaling of energy as function of coordination number [19] and, specifically, that the depth of the pair potential of *n*-coordinated metal atoms, D_n, goes roughly as $n^{-1/2}$ [20]. This simple idea gives surface energies of roughly $0.13E_c$ per atom for fcc(111) and $0.18E_c$ per atom for fcc(100), in excellent agreement with the empirical relation $\gamma = 0.16\ \Delta H_{sub}$ between the surface tension and heat of sublimation of metals [1].

The SMP has very few parameters and they are obtained almost directly from experiment. Such a simple and robust method is satisfying because it should give a similar level of accuracy in a wide range of systems, and cases where it fails can be understood from what is missing in the underlying model; i.e. by having few parameters, we make it unlikely that the fitting process will artificially correct flaws of the model in some systems but not in others. The details of the SMP and its performance for a number of test cases are given elsewhere [21]. We only want to make a few comments here. Firstly, the long-range part of the SMP is cut off by multiplying by $f(r_{ij})$ (Eq. (6)) to keep the model simple and enforce correct surface energies and other properties. This can be viewed as a crude way of 'screening' interactions. It gives an unphysical behavior in the dissociation limit of any system. But it does not cause any problem as long as we limit ourselves to structures near energy minima, as we do here, and there is a simple solution (taking cut-off limits C_1 and C_2 that depend on local geometry) if the long-range part of the potential part matters [21]. Secondly, the SMP gives surface energies that agree with the best embedded atom and effective medium methods [21,22]. It fails to reproduce the finer details of energy as a function of cluster size because there is no information about orbital symmetry, spin-subshells, and other quantum effects. But, these quantum effects become less important as clusters get bigger. We think that, for 55-atom clusters, the SMP method can produce physically meaningful results about some aspects of structure, and produce plausible candidate structures for future studies by more accurate methods. Thirdly, there is nothing in the SMP model about ionic bonding, and adding a purely electrostatic term to the energy U_{el}, which we describe in the next section, significantly improves the binding energies and geometries in mixed metal diatomics and small bimetallic clusters.

2.2. Electronegativity equalization

The SMP is very similar to empirical Gupta-like potentials and embedded-atom methods, which have been used in previous theoretical studies of the structure of bimetallic clusters [23]. The interactions are sums of attractive and repulsive exponential functions of interatomic distance, but each pair interaction depends on the environment so they are not strictly pairwise additive potentials, and the cohesive energy scales roughly as the square-root of the coordination in all these models. But the SMP and Gupta-like potentials, as well as different variants of the embedded-atom method [22], neglect charge transfer and the resulting ionic contribution to the energy. These ionic contributions favor mixing of elements with different electronegativities and could be important in mixed AgAu clusters [24].

We calculate an electrostatic energy as a sum of Coulombic interactions between screened atomic charges plus the energy for charging the atoms:

$$U_{el} = \sum_i \sum_{j>i} J_{ij} Q_i Q_j + \sum_i (U(Q_i) - U(0)) \tag{7}$$

The atomic charges Q_i and screening function J_{ij} depend on the nuclear configuration, and the electronegativity $\chi_i^0 = -(\partial U/\partial N)_v = (\partial U/\partial Q)_v$ and absolute hardness [25] $\eta_i^0 = (1/2)(\partial^2 U/\partial N^2)_v$ of the elements in the system. The electronegativity and absolute hardness are coefficients in the first two terms of a power series expansion of the energy as a function of net charge in a system. For an atom '*a*':

$$\begin{aligned} U(Q_a) &= U(0) + \chi_a^0 Q_a + \eta_a^0 Q_a^2 + \frac{1}{6}\left(\frac{\partial^3 U}{\partial Q_a^3}\right) Q_a^3 \\ &\quad + \frac{1}{24}\left(\frac{\partial^4 U}{\partial Q_a^4}\right) Q_a^4 + \cdots \\ &= U(0) + \chi_a^0 Q_a + (\eta_a^0 + c_3 Q_a + c_4 Q_a^2) Q_a^2 + \cdots \\ &= U(0) + \chi_a^0 Q_a + \eta_a'(Q_a) Q_a^2 + \cdots \end{aligned} \tag{8}$$

In our implementation we retain all powers up to the fourth, which is equivalent to using a charge-dependent value of hardness as the second and third lines of Eq. (8) suggest. The screening function that we use was proposed by Louwen and Vogt [26]:

$$J_{ij} = (R_{ij}^3 + \gamma_{ij}^{-3})^{-1/3} \tag{9}$$

$$\gamma_{ij} = 2(\eta_i^0 \eta_j^0)^{1/2} \tag{10}$$

It correctly reduces to $1/R_{ij}$ in the limit of large distances and to twice the average of the two atoms' hardnesses in the limit of very small distances.

The essential idea of the EE method is that there is only one global electronegativity in a *N*-atom system. If we take the view that individual atoms exist within a *N*-atom system ('atoms-in-molecule' or AIM), then the electronegativity of those AIMs must equalize as the *N*-atom system forms. If we assign individual electronegativities χ_i and hardnesses η_i to every AIM, we can write a system of $(N-1)$ equations: $\chi_i = \chi_1$, $(i = 2,N)$. Charge conservation gives another equation: $\sum_i Q_i = Q_{total}$. This leads to a system of *N* equations with *N* unknowns, the AIM charges Q_i, which we solve by standard methods. There is one important difference between our implementation of EE and that of Rappe and Goddard [27]. Instead of truncating Eq. (8) at the quadratic term and using constants for the AIM hardnesses, we let the hardness of each AIM depend on its charge, $\eta_i = \eta_i(Q_i)$. This gives more

accuracy and avoids unphysical results like charges larger than $+1$ (or even $+3$) for Li atoms in some systems where there are large electronegativity differences between some atoms. In previous work, unphysical charges were prevented by constraining Q_i's to fall within a preset range (for example, $Q_i \geq -2$ for oxygen atoms). In our scheme, the coefficient c_3 and c_4 make the effective hardness η'_a larger as an atom's charge increases. This is intuitively correct, for instance, Li^+ is much harder than Li. The main drawback is that we must solve the system of N equations iteratively to self-consistency because the effective hardnesses depend on the AIM charges, which are initially unknown. But this is not a big problem. A simple mixing scheme almost always delivers self-consistent charges in 20 or fewer iterations. More details about our implementation of EE and its performance in test cases are available on request [28] and will be published elsewhere. Adding EE to SMP decreases the error on the calculated equilibrium bond lengths and dissociation energies in almost every case of heteronuclear metal diatomic molecules that we studied. It brings atomization energies for a series of Ag_5Li_5 isomers in closer agreement to DFT results. And it produces the correct trend in ionization potentials of metal clusters as a function of size and cluster geometry, but it overestimates DFT results typically by 10–20% and, not surprisingly, it fails to reproduce oscillations due to electronic shells and spin subshells. We are not aware of other potentials for metal alloys that include a dynamic charge model to estimate ionic contributions to the energy, as we have here, but we believe that this is essential to describe segregation and ordering in metallic alloys, especially when elements have very different electronegativities.

2.3. Geometry optimization

We performed simulated annealing (SA) optimizations to find the lowest energy substitutional isomers of $A_nB_{(55-n)}$. Each step of our SA runs can be decomposed as follows: (i) interchange the positions of an atom of A and an atom of B; (ii) do a conjugate gradient (CG) optimization, with forces calculated by finite difference; (iii) compare the new energy U_{new} to the previous U_{old} and either reject the new geometry if $U_{new} > U_{old}$ and $\lambda > \exp((-U_{new}+U_{old})/kT)$, where λ is a uniformly distributed random variable in [0,1] and T is the system's temperature, or accept the new geometry. In Monte Carlo simulations we found that our clusters have a melting point of approximately 1300 K. In optimization runs, we typically varied the temperature between 2000 and 200 K. In our case, atom interchange is much more preferable than the usual SA move (small random displacement of one or several atoms) because it brings the system to a new valley of the energy surface nearly every time. Doing CG at every step is necessary when atoms A and B have very different sizes, otherwise many steps would get rejected even when they go to a deep valley because they end up far from the minimum of that valley. Combining CG and SA with atom interchange allows jumps over large energy barriers. So, unlike a SA based on small random atomic displacements, it is possible to find the global minimum even if the initial temperature is less than the melting point. The SA only sees a subset of configurations, the local minima. Its purpose is to solve a discrete optimization problem for which it is well suited. As the optimization progresses, we save every newly accepted structure and eventually write it to a file. In the end, we report the best structure ever found in the SA/CG run, not the last. The other energy minima are also saved to file so they can later be analyzed for correlation between structural features and energy. A typical SA/CG run consisted of a loop over 100 different temperatures from 2000 to 100 K. We required 50 accepted SA/CG moves at each temperature for a total of roughly 5000 accepted moves. In SA, not every attempted move gets accepted: typically, 40% of all attempted moves got accepted. Each move required a CG optimization with numerical energy derivatives, which required on the order of 2000 energy evaluations on average. So, the total number of energy evaluations in one SA/CG run was on the order of 2.5×10^7.

3. Results and discussion

3.1. Energy and structure descriptors

We define a 'relative atomization energy', E, to make comparisons between clusters of different compositions,

$$E(A_xB_y) = \frac{U(A_xB_y)}{xE_c(A) + yE_c(B)} \tag{11}$$

where $U(A_xB_y)$ is the calculated atomization energy of the cluster and $E_c(A)$ is the experimental cohesive energy for element A. We will also report relative isomer energies, which are simply the energy difference between an isomer of A_xB_y and the global minimum energy for the same composition.

In order to compare structures, we calculate three descriptors that express different aspects of mixing. First, we calculate D_{AB} which is just the distance between the center of mass of atoms of type A and the center of mass of atoms of type B, in Å. A large D_{AB} indicates that A and B are separated on a large scale. Second, we calculate a weighted mean distance for pairs of unlike atoms,

$$d_{AB} = \frac{\sum_{i,j}(d_{ij})^{1-n}}{\sum_{i,j}(d_{ij})^{-n}} \tag{12}$$

and a similar weighted mean distance for pairs of like atoms, d_{XX}. Then we obtain a relative comparison of typical AB distances vs AA and BB distances by taking

$$\Delta_{AB} = 2\frac{d_{AB}-d_{XX}}{d_{AB}+d_{XX}} \tag{13}$$

We used $n=4$ in Eq. (12) because it emphasizes short distances and expresses short-range order making Δ_{AB} complementary to D_{AB}. Third, we define the surface enrichment S in the least abundant component as follows. Take a N-atom cluster with N_A atoms of type 'A', N_s surface atoms, N_i interior atoms, and $N_{s,A}$ surface atoms of type A. If the surface composition was

the same as the overall composition, we would have $N_{s,A} = N_A(N_s/N) \equiv \bar{N}_{s,A}$. We compare $N_{s,A}$ to $\bar{N}_{s,A}$ and scale it to get an index S that varies between -1 and $+1$.

$$S = \frac{N_{s,A} - \bar{N}_{s,A}}{|M_{s,A} - \bar{N}_{s,A}|} \tag{14}$$

where $M_{s,A}$ is the maximum possible value of $N_{s,A}$, $M_{s,A} = \mathrm{Min}\{N_A, N_s\}$, when $N_{s,A} > \bar{N}_{s,A}$, and its minimum value, $M_{s,A} = \mathrm{Max}\{0, N_A - N_i\}$, when $N_{s,A} < \bar{N}_{s,A}$. We have $S > 0$ when the surface is richer in A than the interior, and $S < 0$ otherwise.

3.2. Lowest energy structures

The lowest energy isomers are shown in Fig. 1 and their descriptors and energy are in Table 1. As expected from surface energies, the Ag atoms segregate to the surface in $Ag_{13}Cu_{42}$, $Cu_{27}Ag_{28}$, and $Cu_{13}Ag_{42}$, and as a result, the latter has full icosahedral symmetry. Twelve of the thirteen Ag atoms form a icosahedron at the surface of $Ag_{13}Cu_{42}$: it is energetically favorable (by 1.06 eV) to put the 13th Ag atom on the surface rather than in the center. The minimum energy structure of $Ag_{12}Cu_{43}$ must surely have the 12 Ag atoms at the surface with I_h symmetry. In $Au_{13}Cu_{42}$ the 13 Au atoms are on the surface,

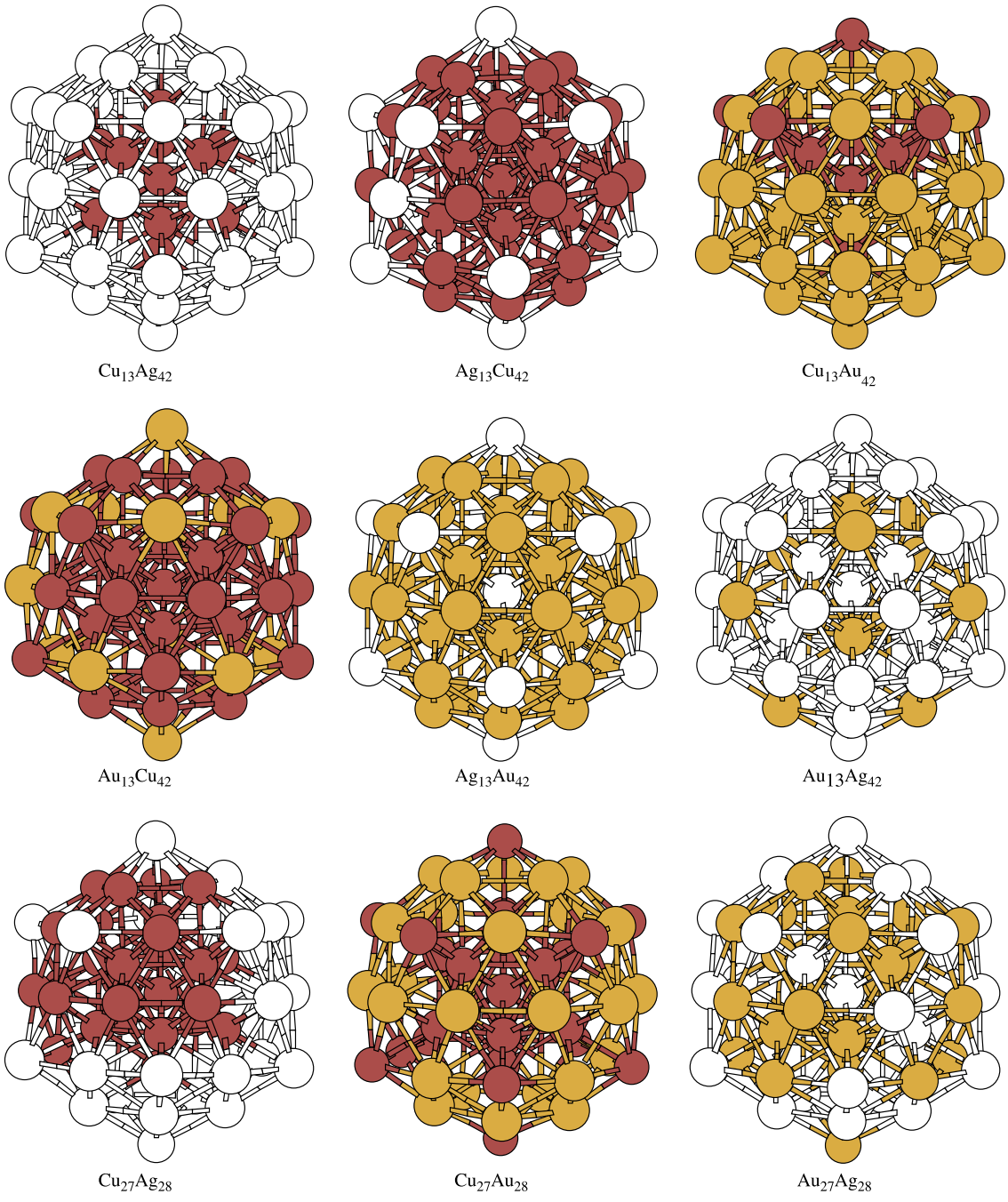

Fig. 1. Lowest energy substitutional isomsers.

Table 1
Descriptors of the lowest energy substitutional isomers of $A_{13}B_{42}$ and a random sample of five structures, scaled cohesive energy (Eq. (11)), and ionization energy (eV)

	D_{AB}	Δ_{AB}	S	E	IE
$Cu_{13}Ag_{42}$	0.01	0.08	−1.00	0.8355	6.42
Sample avg	0.93	0.00	−0.56		
Rmsd	0.43	0.03	0.20		
$Ag_{13}Cu_{42}$	0.43	0.07	1.00	0.8333	6.53
Sample avg	1.02	0.08	1.00		
Rmsd	0.28	0.01	0.00		
$Cu_{13}Au_{42}$	1.99	−0.04	−0.40	0.8398	7.39
Sample avg	0.79	−0.04	−0.27		
Rmsd	0.32	0.01	0.08		
$Au_{13}Cu_{42}$	0.44	0.01	1.00	0.8470	7.19
Sample avg	0.95	0.04	0.87		
Rmsd	0.26	0.01	0.26		
$Ag_{13}Au_{42}$	0.00	−0.03	0.67	0.8413	6.80
Sample avg	1.26	−0.01	0.41		
Rmsd	0.36	0.02	0.24		
$Au_{13}Ag_{42}$	0.18	−0.08	−0.29	0.8450	6.40
Sample avg	0.84	−0.04	−0.29		
Rmsd	0.38	0.01	0.14		

but unlike Ag atoms in $Ag_{13}Cu_{42}$, Au atoms preferentially take the edge-capping, or 'e', positions. There are 42 surface atoms in the 55-atom Mackay icoshedron, 12 are atom-capping, or 'a', and have a coordination of 6, and 30 are 'e' and have a coordination of 8. To explain the structure of $Au_{13}Cu_{42}$, we must consider both the surface energy [1] (1.67 J m^{-2} for Cu, 1.14 J m^{-2} for Ag, 1.41 J m^{-2} for Au) and the cohesive energy (3.49 eV for Cu, 2.95 eV for Ag, 3.81 eV for Au). The Au atoms segregate to the surface because Cu has a higher surface energy; however, Au has the higher cohesive energy, so it takes the surface sites 'e' because those have the highest coordination. Within those constraints, the Au atoms stay as far from each other as possible ('AB ordering') because they all carry charges of the same sign. Since Ag has a lower cohesive energy than Cu, Ag atoms occupy the 'a' surface sites in $Ag_{13}Cu_{42}$.

The C_{5v} symmetry structure of $Cu_{13}Au_{42}$ is the result of competing factors. The high surface energy of Cu favors interior sites for Cu atoms, but the ionic energy term favors putting Cu atoms away from each other. The lowest energy structure is a compromise. It has seven Cu atoms in the interior and six Cu atoms on the surface, all of them at 'a' sites in line with the lower cohesive energy of Cu vs Au. By comparison, the structure with 13 interior Cu atoms is higher in energy by 1.17 eV. The EE term of the energy is much smaller than the SMP term, it varies between roughly 1 and 5 eV compared to roughly $55 \times 0.85 \times 3.2 = 150$ eV for SMP in these clusters. But, as $Cu_{13}Au_{42}$ shows, the EE energy term strongly affects the relative energies of structures. In $Au_{13}Cu_{42}$ the 13 Au atoms are at the surface, and two of them occupy 'a' surface sites at opposite end. The remaining 11 Au atoms are all at 'e' sites, and ten of those are arranged as staggered pentagons. We can describe the arrangement of Au and Cu atoms on the surface, layer by layer, by listing a series of (N_{Au}s,N_{Cu}s′), where N_{Au} is the number of Au atoms in the layer, and s is the site (a or e) they occupy: (1a,0)/(0,5e)/(5a,5e)/(1e,9(4e+5a))/(5e,5a)/(0,5e)/(1a,0). There are only two nearest-neighbor Au–Au pair and they both involve the Au atom in the 4th layer. If we replaced that atom by a Cu atom, we would get a I_h structure that is surely the global minimum of $Au_{12}Cu_{43}$ in our model. The maximum separation of the Au atoms shows up as a small value of D_{AB} in Table 1.

The lowest energy $Ag_{13}Au_{42}$ has I_h symmetry, with a central Ag atom and the remaing twelve Ag atoms at 'a' surface sites. Putting a Ag atom in the center decreases $|U_{SMP}|$, but it increases the number of Ag–Au nearest-neighbour pairs and therefore increases $|U_{EE}|$, and the net effect is a decrease in energy. But things are different for $Ag_{13}Cu_{42}$: we did a local optimization for the I_h structure and found it gave an energy higher than the global minimum by 1.35 eV. The reason for the difference is the strain on the central atom. In a 13-atom icosahedron the central-to-surface interatomic distance is 4% smaller than the surface-to-surface interatomic distance; the radial compression is almost the same between the next two shells of the 55-atom icosahedron. Therefore, the interior atoms of an icosahedron are compressed. The resulting strain energy in I_h $Ag_{13}Au_{42}$ is small because Ag and Au have comparable bulk nearest-neighbour distances (R_{nn} = 2.89 Å for Ag, R_{nn} = 2.88 Å for Au), but the strain energy in I_h $Ag_{13}Cu_{42}$ is large because Ag is much larger than Cu (R_{nn} = 2.56 Å for Cu).

The minimum of $Au_{13}Ag_{42}$ is another structure that is a compromise between competing effects. Its surface is richer in Ag, but seven of the Au atoms prefer the 'e' sites on the surface over the remaining interior sites. The rather large electronegativity difference between Ag and Au is what drives some Au atoms to the surface to increase Ag–Au mixing.

$Cu_{27}Ag_{28}$ is strongly segregated as Fig. 1 shows, and the large values of D_{AB} and Δ_{AB} in Table 2 confirm this. By comparison, the Δ_{AB} value for $Cu_{27}Au_{28}$ (0.01) is close to zero, which is characteristic of a random alloy, and the value for $Au_{27}Ag_{28}$ (−0.08) is characteristic of AB ordering. The electronegativity difference is mainly what favors structures with smaller Δ_{AB} (mixing, or AB ordering). The larger value of Δ_{AB} for $Cu_{27}Au_{28}$, compared to $Au_{27}Ag_{28}$, results from the strong preference of Cu for interior sites, and this is because Cu has a higher surface energy than Au and a smaller size that relieves the compression in the interior of the icosahedron.

Table 2
Descriptors of the lowest energy substitutional isomers of $A_{27}B_{28}$ and a random sample of five structures, scaled cohesive energy (Eq. (11)), and ionization energy (eV)

	D_{AB}	Δ_{AB}	S	E	IE
$Cu_{27}Ag_{28}$	2.22	0.12	−1.00	0.8364	6.46
Sample avg	1.11	0.06	−0.85		
Rmsd	0.55	0.02	0.14		
$Cu_{27}Au_{28}$	0.54	0.01	−1.00	0.8500	7.36
Sample avg	0.75	−0.01	−0.70		
Rmsd	0.23	0.03	0.17		
$Au_{27}Ag_{28}$	0.29	−0.08	−0.40	0.8490	6.67
Sample avg	0.92	−0.03	−0.37		
Rmsd	0.38	0.01	0.15		

Details of the structures are complicated because 27 (or 28) does not add up to any simple combination of sites, but in all three structures the element with lowest cohesive energy prefers the 'a' surface sites, and this in turn leads to the formation of layers at the surface of many cluster. This is most clearly seen in $Cu_{27}Au_{28}$ maybe. If we orient the cluster to put a 'a' site at the top, we see a sequence of layers with these (Cu,Au) compositions: (1a,0)/(0,5e)/(5a,5e)/(1e,9e)/(5a,5e)/(1e,4e)/(1a,0). The 3rd and 5th layers have a perfect alternating pattern which is favored both by coordination (6 for Cu at 'a' sites, 8 for Au at 'e' sites) and by Coulombic interactions. The energy differences between different choices for the positions of the remaining two Cu atoms are relatively small. The $Cu_{25}Au_{30}$ cluster composition, with I_h symmetry structure, would have extra stability in our model.

3.3. Trends in structures and energies

To help in making comparisons, we picked five structures at random from each optimization runs. The average and root-mean-square deviation of their descriptors are shown in Tables 1 and 2 in the second and third line for each cluster composition. A typical value of D_{AB} for these random structures is 1.0 Å. Using this as a criterion, two clusters show segregation on a large scale, $Cu_{13}Au_{42}$ ($D_{AB}=1.99$) and $Cu_{27}Ag_{28}$ ($D_{AB}=2.22$). These two clusters are quite different if we look at Δ_{AB}: $Cu_{13}Au_{42}$ shows short-range AB ordering (a negative $\Delta_{AB}=-0.04$) while $Cu_{27}Ag_{28}$ shows segregation at short range (positive $\Delta_{AB}=+0.12$). The Δ_{AB} values of the random structures vary typically between -0.05 and $+0.05$. Generally, $Ag_{13}Cu_{42}$ structures are characterized by short-range segregation. The lowest energy structures of $Au_{13}Ag_{42}$ and $Au_{27}Ag_{28}$ have the most negative Δ_{AB}, indicative of AB ordering. One expects that Δ_{AB} and S will tend towards zero at higher temperatures. Although our sampling of structures is crude and does not correspond to any temperature, we see the expected trend as we go from the lowest energy structures to random structures. However, S generally stays closer to the value it has in the lowest energy structure for most cluster compositions, which suggests significant surface enrichment even at high temperatures.

The work functions of the three metals are all approximately 4.3 eV. Our calculated ionization energies (IEs, Tables 1 and 2) are larger than that, and somewhat larger than those of smaller clusters [29]. The IEs correlate with the electronegativity of the metals, which follow the increasing order $\chi(Cu)\approx\chi(Ag)<\chi(Au)$, so they increase with Au content. Besides this trend, the differences between the calculated IEs are probably too small to be meaningful.

Looking at the lowest energy structures, the average of the scaled cohesive energies are 0.8350 for the three CuAg clusters, 0.8456 for CuAu clusters, and 0.8451 for AgAu clusters. So, within our model, mixing metals with substantially different electronegativities (CuAu or AgAu) gives cohesive energies higher by roughly 1% compared to the case with very similar electronegativities (CuAg). In relative terms, the stabilizing effect of charge transfer is more pronounced in clusters with composition near 50–50%. For other compositions, the stabilizing effect of charge transfer is more pronounced in clusters that are richer in the least electronegative element ($Au_{13}Cu_{42}$ and $Au_{13}Ag_{42}$).

4. Conclusions

We used an empirical potential and obtained the lowest energy substitutional isomers of 55-atom Mackay icosahedra bimetallic clusters. Our empirical potential has two contributions: a (covalent) scaled Morse potential U_{cov} that depends on coordination and interpolates between the experimental properties of diatomic and bulk metals, and a ionic term U_{el} associated with the charging and Coulombic interactions of AIMs. Although U_{el} is much smaller in magnitude than U_{cov}, it plays a crucial role. Some of our general findings about the favored structures relate to features in U_{cov}, namely: the metal with lowest surface energy (particularly Ag) segregates to the surface; the metal with lowest cohesive energy occupies in priority the 'a' sites at the surface; the larger atoms are generally not found in the interior because of the radial compression in icosahedra. Other general aspects of favored structures relate to U_{el}, namely: short-range AB ordering is prevalent in mixtures of metals where the difference of electronegativities, $\Delta\chi_{AB}$, is sufficiently big, especially AgAu where the two elements have similar atomic radii; surface energy and ionic energy compete and can lead to 'structures of compromise' like $Cu_{13}Au_{42}$ and $Au_{13}Ag_{42}$ that have only partial surface enrichment. The cohesive energies are roughly 1% larger as a result of charge transfer in cases where $\Delta\chi_{AB}\approx 0.40$ (Pauling's scale).

The structures that we considered in our search are all based on the Mackay icosahedron, but otherwise, the low energy structures we found are the result of an extensive global optimization. The Mackay icosahedron is likely to be the global minimum of 55-atom metallic clusters [13–15], so we believe that we would reach the same conclusions about mixing and surface segregation if we did a search among all possible structures.

Apart from test cases [28], this is the first application of the SMP-EE energy model to bimetallic systems. Some technical aspects of SMP-EE need improvement to make calculations faster, but the time per SMP-EE energy evaluation (roughly 0.005 s. on a Pentium PC) in 55-atom systems is already promising. In future work, we plan to study the bimetallic clusters CuAg, CuAu, and AgAu over a wider range of size and compositions, and carry Monte Carlo simulations at temperatures comparable to those at which catalysts operate. The structure of smaller bimetallic clusters is generating much interest [23]. By combining SMP-EE with a global optimization method [22] we should be able to discover plausible low energy structures and study the effect of charge transfer on cluster structure. The electronic structure of these bimetallic systems presents a serious challenge, which has been tackled only for relatively small clusters up to now (see for example [24]). If structure optimization is done by SMP-EE, one avoids

most of the computing cost of a full DFT calculation. This way, it should be possible to characterize the electronic structure of a few representative bimetallic clusters of moderately large size and relevant to catalysis. This would bring up many more questions, and answers, about bimetallic clusters, than we could bring up here.

Acknowledgements

This work was supported by the Natural Sciences and Engineering Research Council of Canada.

References

[1] G.A. Somorjai, Introduction to Surface Chemistry and Catalysis, Wiley, New York, 1994.
[2] O.S. Alexeev, B.C. Gates, Ind. Eng. Chem. Res. 42 (2003) 1571 and references therein.
[3] J.M. Thomas, R. Raja, B.F.G. Johnson, S. Hermans, M.D. Jones, T. Khimyak, Ind. Eng. Chem. Res. 42 (2003) 1563 and references therein.
[4] C.J.H. Jacobsen, S. Dahl, B.S. Clausen, S. Bahn, A. Logadottir, J.K. Nørskov, J. Am. Chem. Soc. 123 (2001) 8404.
[5] R.W.J. Scott, C. Sivadinarayana, O.M. Wilson, Z. Yan, D.W. Goodman, R.M. Crooks, J. Am. Chem. Soc. 127 (2005) 1380.
[6] J.H. Sinfelt, Bimetallic Catalysts: Discoveries, Concepts, and Applications, Wiley, New York, 1983; J.H. Sinfelt, Catal. Lett., 9159.
[7] J.R. Chelikowsky, Surf. Sci. 139 (1984) L197.
[8] A.V. Ruban, H.L. Skriver, J.K. Nørskov, Phys. Rev. B 59 (1999) 15990; M. Aldén, I.A. Abrikosov, B. Johansson, N.M. Rosengaard, H.L. Skriver, Phys. Rev. B 50 (1994) 5131; M. Aldén, H.L. Skriver, B. Johansson, Phys. Rev. B 50 (1994) 12118; M. Aldén, B. Johansson, H.L. Skriver, Phys. Rev. B 51 (1995) 5386.
[9] S. Müller, J. Phys.: Condens. Matter 15 (2003) R1429; M.H.F. Sluiter, Y. Kawazoe, Phys. Rev. B 71 (2005) 212201.
[10] J. Farges, M.F. De Feraudy, B. Raoult, G. Torchet, Adv. Chem. Phys. 70 (Part 2) (1988) 45; T.D. Klots, B.J. Winter, E.K. Parks, S.J. Riley, J. Chem. Phys. 92 (1990) 2110; E.K. Parks, L. Zhu, J. Ho, S.J. Riley, J. Chem. Phys. 100 (1994) 7206; J. Akola, M. Manninen, H. Häkkinen, U. Landmann, X. Li, L.-S. Wang, Phys. Rev. B 60 (1999) R11297; T.M. Briere, M.H.F. Sluiter, V. Kumar, Y. Kawazoe, Phys. Rev. B 66 (2002) 064412; J. Wan, R. Fournier, J. Chem. Phys. 119 (2003) 5949; H.-J. Zhai, J. Li, L.-S. Wang, J. Chem. Phys. 121 (2004) 8369.
[11] U. Röthlisberger, W. Andreoni, P. Giannozzi, J. Chem. Phys. 96 (1992) 1248; V. Kumar, Y. Kawazoe, Phys. Rev. B 65 (2002) 125403; Y.-C. Bae, H. Osanai, V. Kumar, Y. Kawazoe, Phys. Rev. B 70 (2004) 195413; R. Fournier, J.B.Y. Cheng, A. Wong, J. Chem. Phys. 119 (2003) 9444.
[12] C.M. Chang, Y.M. Chou, Phys. Rev. Lett. 93 (2004) 133401.
[13] T.P. Martin, T. Bergmann, H. Göhlich, T. Lange, Chem. Phys. Lett. 176 (1991) 343; E.K. Parks, T.D. Klots, B.J. Winter, S.J. Riley, J. Chem. Phys. 99 (1993) 5831; B.J. Winter, E.K. Parks, S.J. Riley, J. Chem. Phys. 94 (1991) 8618; W. Vogel, B. Rosner, B. Tesche, J. Phys. Chem. 97 (1993) 11611–11616; W. Vogel, D.G. Duff, A. Baiker, Langmuir 11 (1995) 401–404.
[14] H.-G. Boyen, A. Ethirajan, G. Kästle, F. Weigl, P. Ziemann, G. Schmid, M.G. Garnier, M. Büttner, P. Oelhafen, Phys. Rev. Lett. 94 (2005) 016804.
[15] C.L. Cleveland, U. Landman, M.N. Shafigullin, P.W. Stephens, R.L. Whetten, Z. Phys. D 40 (1997) 503Â; J.A. Ascencio, C. Gutiérrez-Wing, M.E. Espinosa, M. Martín, S. Tehuacanero, C. Zorrilla, M. José-Yacamán, Surf. Sci. 396 (1998) 349.
[16] T.P. Martin, Phys. Rep. 273 (1996) 199 and references therein
[17] P. Morse, Phys. Rev. 34 (1929) 57; M. Dagher, H. Kobeissi, M. Kobressi, J. D'Incan, C. Effantin, J. Comput. Chem. 14 (1993) 1320.
[18] J.H. Rose, J. Ferrante, J.R. Smith, Phys. Rev. Lett. 47 (1981) 675.
[19] A.R. Miedema, K.A. Gingerich, J. Phys. B: Atom. Mol. Phys. 12 (1979) 2081.
[20] M. Methfessel, D. Hennig, M. Scheffler, Appl. Phys. A 55 (1992) 442.
[21] R. Fournier, M. Zhang, Y. Soudagar, M. Hopkinson, in: T. Simos, G. Maroulis (Eds.), Lecture Series on Computer and Computational Sciences, VSP International Science Publishers, The Netherlands, submitted for Publication.
[22] S.B. Sinnott, M.S. Stave, T.J. Raeker, A.E. DePristo, Phys. Rev. B 44 (1991) 8927.
[23] M.J. López, P.A. Marcos, J.A. Alonso, J. Chem. Phys. 104 (1996) 1056; S. Darby, T.V. Mortimer-Jones, R.L. Johnston, C. Roberts, J. Chem. Phys. 116 (2001) 1536.
[24] V. Bonacíć-Koutecký, J. Burda, R. Mitrić, M. Ge, G. Zampella, P. Fantucci, J. Chem. Phys. 117 (2002) 3120.
[25] R.G. Parr, W. Yang, Density Functional Theory of Atoms and Molecules, Oxford University Press, Oxford, 1989.
[26] J.N. Louwen, E.T.C. Vogt, J. Mol. Catal. A134 (1998) 63.
[27] A.K. Rappe, W.A. Goddard III, J. Phys. Chem. 95 (1991) 3358.
[28] Min Zhang, Graduate Research Report. York University, 2004.
[29] C. Jackschath, I. Rabin, W. Schulze, Z. Phys. D: At., Mol. Clusters 22 (1992) 517.
[30] J. Cheng, R. Fournier, Theor. Chem. Acc. 112 (2004) 7.
[31] S.-Y. Wang, J.-Z. Yu, H. Misuseki, J.-A. Yan, C.-Y. Wang, J. Chem. Phys. 120 (2004) 8463.
[32] O.D. Häberlen, S.-C. Chung, M. Stener, N. Rösch, J. Chem. Phys. 106 (1997) 5189.